Crystalline Corrugation in Multilayer Films on Aqueous Subphases

by **R. Buller**[a]), **I. Weissbuch**[a]), **S. Cohen**[a]), **K. Kjaer**[b]), **M. Lahav**[a]), and **L. Leiserowitz***[a])

[a]) Department of Materials and Interfaces, Weizmann Institute of Science, Rehovot 76100, Israel
[b]) Material research Department, Risø National Laboratory, DK-4000 Roskilde

Dedicated to Professor *Jack D. Dunitz* on the occasion of his 80th birthday

A strong *Bragg* peak, attributed to regular corrugation in a crystalline film, was detected in a series of self-assembled supramolecular complexes of bifunctional bolaamphiphiles of different lengths, with divalent ions of Pb and Cu, at the air–aqueous interface. This peak has a *d* spacing half that of the proposed corrugation-repeat length of *ca.* 82 Å, which is not a multiple of the long lattice spacing of the crystalline structure, and is susceptible to film compression. This corrugation is interpreted in terms of unfavorable interactions between the polar aqueous surface and the nonpolar hydrocarbon part of the bolaamphiphiles. To establish the nature of the corrugation, grazing-incidence X-ray diffraction and specular X-ray reflectivity with synchrotron radiation were applied, as well as scanning force microscopy of films deposited on mica.

1. Introduction. – Physical, electronic, and catalytic properties of materials are largely determined by the structure and texture of the surfaces that delineate them [1]. This is particularly true for nanomaterials and thin films, as well as other meso-structures having high surface-to-bulk ratios. Thin organic films can assume a corrugated texture formed spontaneously or as a result of applied stress.

Corrugated-superstructure determination has been reported for lyotropic [2] and smectic liquid crystals [3] making use of X-ray diffraction, as well as on their film counterparts by scanning force microscopy (SFM) [4].

With the advent of intense and highly parallel X-rays from synchrotron sources, it has become possible in recent years to probe the structures of crystalline thin films at the air–aqueous solution interface, by grazing-incidence X-ray diffraction (GIXD) and specular X-ray reflectivity (XR). These methods provide information not only on the crystalline structure of the thin films, but also on their size and surface texture.

More recently, X-ray surface scattering studies on *Langmuir* monolayers on $CdCl_2$ aqueous solution at high pH [5][6], octadecyltrichlorosilane [7], and various poly((*tert*-butyl)-styrene)–(polystyrene)-sulfonate block copolymers [8] demonstrated the formation of corrugation with a wavelength ranging from 200 to 2000 Å. Regular corrugation in monolayers on solid supports has been imaged, mainly by SFM [9] and scanning tunneling microscopy [10], revealing wave or saw-tooth structures.

Here, we report the formation of multilayer crystalline self-assemblies that display regular corrugation, as analyzed by GIXD, XR, and SFM.

1.1. *The Crystalline Multilayers.* Recently, we have investigated the self-assembly of a series of bifunctional bolaamphiphiles, in enantiomerically pure (*l*) and racemic (*dl*) forms (labeled C_{22}Lys or C_{22}Orn, shown in *Fig. 1,a*) in aqueous solution containing divalent ions of Pb and Cu. These molecules form three-component organo-metallic

complexes in crystalline multilayer domains of *ca.* 40 (±10) Å thickness, having $[C_{22}Orn]_2CuPb$ or $[C_{22}Lys]_2CuPb$ stoichiometry [11]. Within these crystalline films, the organic molecules lie with their long axes parallel to the H_2O surface, and the Cu^{2+} and Pb^{2+} metal ions are arranged in alternating sheets perpendicular to the plane of the solution surface, separated by the organic spacer molecules, as viewed parallel and perpendicular to the solution surface (*Fig. 1*, *b* and *c*). Interestingly, we observe, in addition to the *Bragg* peak of the crystalline lattice, a strong peak, designated henceforth as the *W* peak (see *Fig. 2*), with *d* spacing that is neither a multiple of the long d_{01} lattice spacing of the crystalline film, nor a precise multiple of the short (*h*,*k*) spacings of the crystalline film.

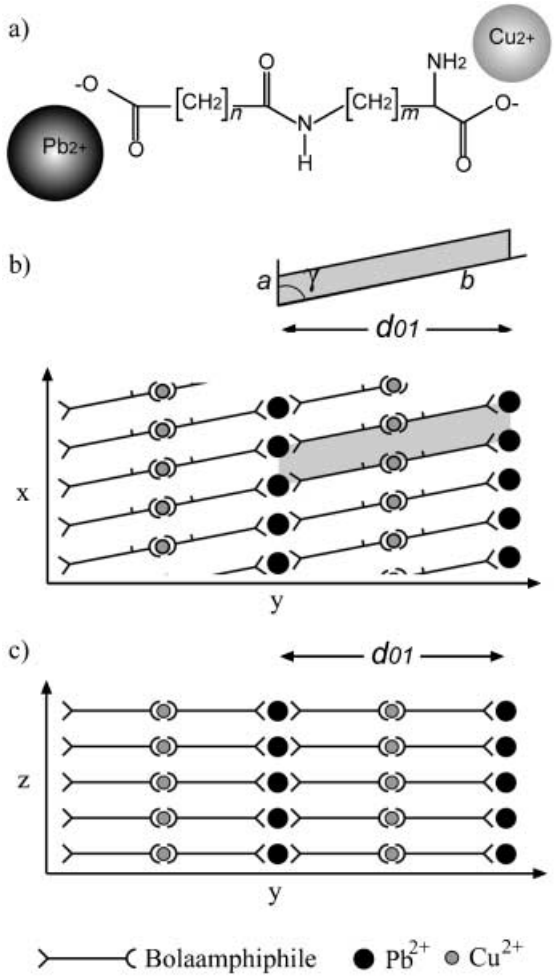

Fig. 1. a) *Bifunctional bolaamphiphiles abbreviated as* $C_{22}Orn$ (for $n=20$ and $m=3$), *and* $C_{22}Lys$ (for $n=20$ and $m=4$). b) c) *Schematic packing arrangements of the bolaamphiphile molecules complexed to two different metal-ion types, viewed perpendicular and parallel to the air–aqueous solution interface.*

An analysis of various structural models that may account for the *W* peak led us to postulate that this reflection arises from a regular corrugation within the film, in a direction parallel to the air–aqueous interface, and perpendicular to the long-chain axis. Here, we present a detailed analysis justifying this postulate.

2. Results and Discussion. – We first investigated the response to film compression, of the intensity, position, and shape of the *W* peak, relative to the *Bragg* peaks arising from the crystalline lattice, *via* a GIXD and XR study performed on the various films at the air–solution interface. The experiments were carried out on the liquid-surface diffractometer at the synchrotron beamline BW1, HASYLAB. A brief description of the methods is given in the *Exper. Part* [12].

2.1. *Grazing-Incidence X-Ray Diffraction (GIXD)*. The GIXD patterns measured from the three-component systems are very similar, a representative thereof being shown in *Fig. 2*. This pattern displays three types of *Bragg* reflection: *a*) one set comprises successive (0,*k*) harmonics observed up to the 10th order, corresponding to the long *d*(0,1) lattice spacing of the two spacer molecules arranged head-to-head and tail-to-tail, and linked *via* intercalating Cu^{2+} and Pb^{2+} metal ions (*Fig. 1*,*b*). These metal ions lie in sheets perpendicular to the solution surface (*Fig. 1*,*c*) in accordance with the shape of the (0,*k*) *Bragg* rods all of which peak at $q_z = 0$ Å^{-1}. Similar GIXD patterns exhibiting many *Bragg* reflection harmonics corresponding to the long spacing were observed in related systems [13][14]. *b*) The other type of reflection arises from the interchain arrangement of the crystalline multilayer, of which the *Bragg* peak with *d* spacing of 4.1 A is the strongest [11]. *c*) Finally, the highly intense *W* peak, with a d_w spacing of *ca.* 41.5 Å, has a *Bragg* rod intensity profile that peaks at $q_z = 0$ Å^{-1} and displays a fast falloff along q_z. Furthermore, we do not observe its higher-order reflections (namely d_W/n, $n = 2, 3$ *etc.*). The d_w spacing, *ca.* 41.5 Å, is not a multiple of the long (0,1) lattice spacing for the various crystalline films (see *Table 1*), nor is d_w a precise multiple of the 4.1 Å interchain spacing. The *Bragg* rod profile of the latter (*Fig. 2*) is skewed along q_t ($= q_{xy}^2 + q_z^2)^{1/2}$. This skewing may be interpreted in terms of the multilayer crystal, bent about a direction parallel to the reciprocal lattice vector *d**(0,1), namely about the *y* axis shown in *Fig. 1*,*b*. A multilayer bent about any other direction parallel to the solution surface would have yielded skewed (0,*k*) *Bragg* rods.

Table 1. *The (0,1) Lattice Spacing and* d-*Spacing* (in Å) *Corresponding to the* W Bragg *Peak from Various Films Measured at the Air–Solution Interface.*

Compound	(0,1) Lattice spacing[a])	*W*-Peak *d* spacing
[(*d*,*l*)-C_{22}Orn]$_2$CuPb	70.2	41.8–40.9[b])
[(*l*)-C_{22}Orn]$_2$CuPb	70.0	42.4–41.7[b])
[(*d*,*l*)-C_{22}Lys]$_2$CuPb	73.3	42.7[c])
[(*l*)-C_{22}Lys]$_2$CuPb	73.2	43.1–42.2[b])

[a]) The lowest observed (0,*k*) reflection is for $k = 2$. [b]) Depending on the compression (see *Fig. 5*,*b* and *c*). [c]) Measured at zero surface pressure only.

There is partial overlap of the *W* peak with the (0,2) peak arising from the crystalline lattice. An accurate estimate of the shape and position of the *W* peak was

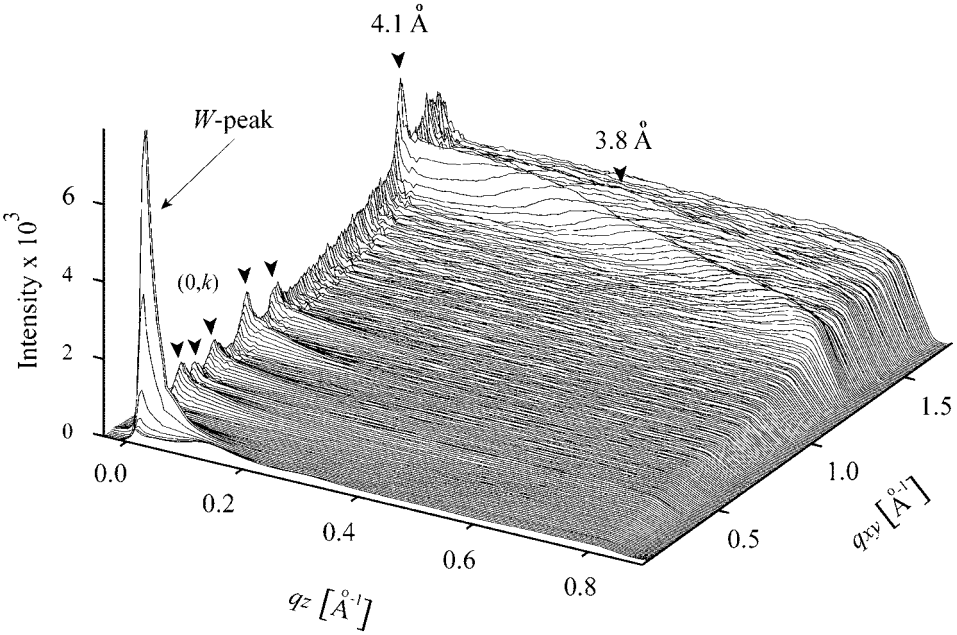

Fig. 2. *2D Surface plot of the scattered X-ray intensity* I(q_{xy},q_z) *showing* Bragg *reflections of [*(d,l)*-C_{22}Lys]$_2$CuPb on aqueous solutions*

obtained by a separation of the intensity profile along q_{xy} (*Fig. 3*,*a*), by least-square fitting. On film compression, the positions of all the (0,*k*) *Bragg* peaks originating from the crystalline long lattice spacing remained unchanged[1]). In contrast, the *d* spacing of the *W* peak, was slightly, but consistently reduced, by *ca.* 1 Å, until reaching a constant value (*Fig. 3*,*c* and *Table 1*)[2]). This behavior is consistent with the steep rise in the surface pressure of the film on reaching maximum compression (*Fig. 3*,*d*). Although the long *b* axis of the complexes [C_{22}Orn]$_2$CuPb and [C_{22}Lys]$_2$CuPb differ by *ca.* 3 Å, there is no corresponding difference in the *d* spacing of the *W* peak.

Upon film compression, the crystalline coherence length (*L*), as calculated from the FWHM(q_{xy}) of the (0,*k*) and the *W Bragg* peaks, increased slightly (see *Table 2*). In contrast, the integrated intensities of the *W Bragg* peak increased more sharply than that of the (0,2) *Bragg* peak (*Fig. 4*). According to the FWHM(q_z) of the *W Bragg* rod, the estimated thickness of the film is 90 Å.

2.2. *Specular X-Ray Reflectivity.* To glean more information on the nature of the film, X-ray-reflectivity (XR) measurements were performed on the same film of [(*l*)-C_{22}Lys]$_2$CuPb from which the GIXD data were obtained. The XR curves provide information on the electron-density profile $\rho(z)$ of the film along the direction normal to the H_2O surface, regardless of its crystallinity. *Fig. 5* shows the specular reflectivity R/R_F as a function of q_z/q_c measured for various points along the π-*A* isotherm. On film

---

[1]) The positions of these *Bragg* peaks yield an average scatter of 0.5 Å in the corresponding *d* spacing.

[2]) The position of the *W Bragg* peak could be determined more accurately, as it is sharper.

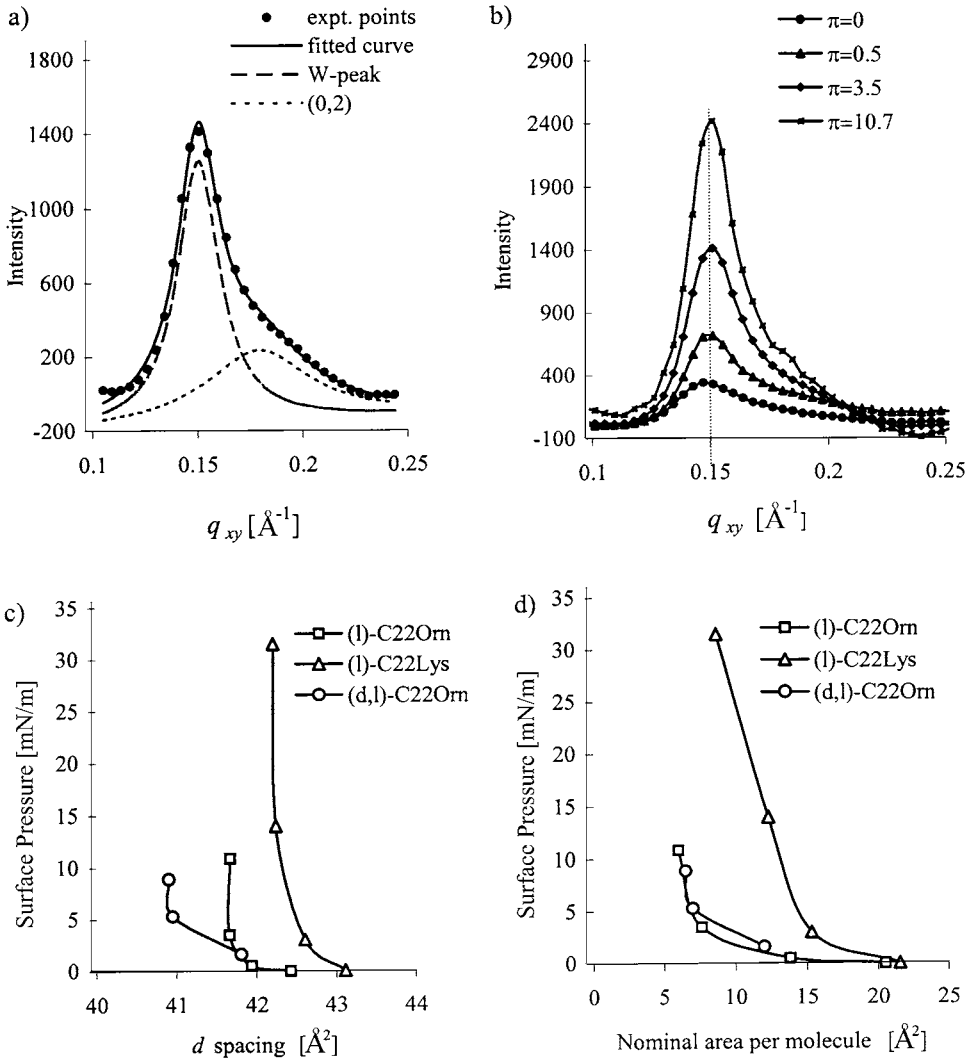

Fig. 3. a) *Curve fitting along* q_{xy}, *in the range 0.1–0.25 Å*$^{-1}$, *of* q_z*-integrated intensities of (0,2) and* W*-peaks, measured from [(l)-C*$_{22}$*Orn]*$_2$*CuPb film on the air–solution interface at* $\pi = 3.5$ *mN/m.* b) q_z*-Integrated intensity in the same* q_{xy} *range, measured from film at various surface pressures along the* π-A *isotherm.* c) *The* d *spacing of the* W*-peak measured from various films at different surface pressures along the* π-A *isotherm.* d) π-A *Isotherms measured from various films showing the points at which the GIXD data were measured.*

compression, we observe a sharp drop in normalized X-ray reflectivity R/R_F, which may be unambiguously interpreted as arising from an increase in molecular-surface roughness [15]. Such an observation has been made for other films for which film buckling was invoked [8].

An estimate of the film thickness and surface roughness was obtained from an analysis of the reflectivity curves. The electron-density profile $\rho(z)$ of the film was

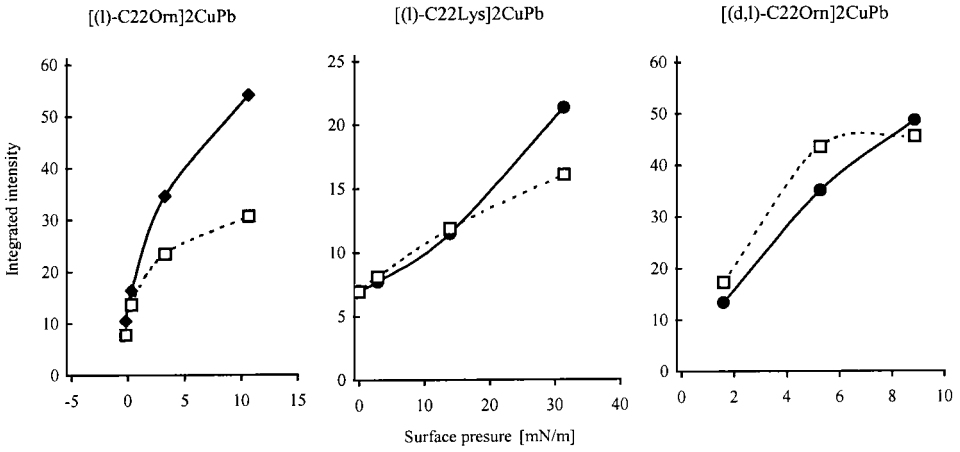

Fig. 4. *Total integrated intensity of the (0,2) and* W-*peak* Bragg *reflections, as measured from various films, as a function of surface pressure*. Experimental data represented by geometric shapes; *W* peak (filled diamonds) and (0,2) peak (open squares).

Table 2. *Crystalline Coherence Lengths*[a]) L (in Å) *Corresponding to the (0,2) Reflection of the Crystalline Lattice, and to That of the* W *Peak, at Various Surface Pressures* π (in mN/m) *of Different Films Measured at the Air–Aqueous Interface*

Compounds	π	0	3	14	31
[(*l*)-C_{22}Lys]$_2$CuPb	L(*W* peak)	270	300	300	310
	L(0,2)	90	100	100	130
	π	0	0.5	3	10
[(*l*)-C_{22}Orn]$_2$CuPb	L(*W* peak)	200	250	250	280
	L(0,2)	90	100	100	100
	π	1.6	5	8	
[(*d*,l)-C_{22}Orn]$_2$CuPb	L(*W* peak)	240	280	260	
	L(0,2)	90	90	100	

[a]) Calculated according to the *Scherrer* formula [16].

expressed in terms of a one-box model, since the molecular complex lies parallel to the H_2O surface (*Fig. 1*, *b* and *c*), where box height corresponds to film thickness. The electron density of the box model was calculated making use of the 2D cell dimensions extracted from the GIXD experiments, and its content of 663 electrons, according to the stoichiometry of the complex [(*l*)-C_{22}Lys]$_2$CuPb. The electron density of the solution subphase is very close to that of pure H_2O (0.334 $e^-/Å^3$). For simplicity, we assumed identical roughening of the film at both its interfaces.

The reflectivity curves could be fitted, provided the film was assumed to consist of 'patches' of three different thicknesses that scatter X-rays incoherently [17]. In the uncompressed state of the film, the (0,*k*) *Bragg* rods gave a crystalline thickness of *ca.* 40 Å, and the *W Bragg* rod of *ca.* 90-Å thickness. These values obtained from the GIXD data barely changed upon film compression. It was also assumed that the disordered

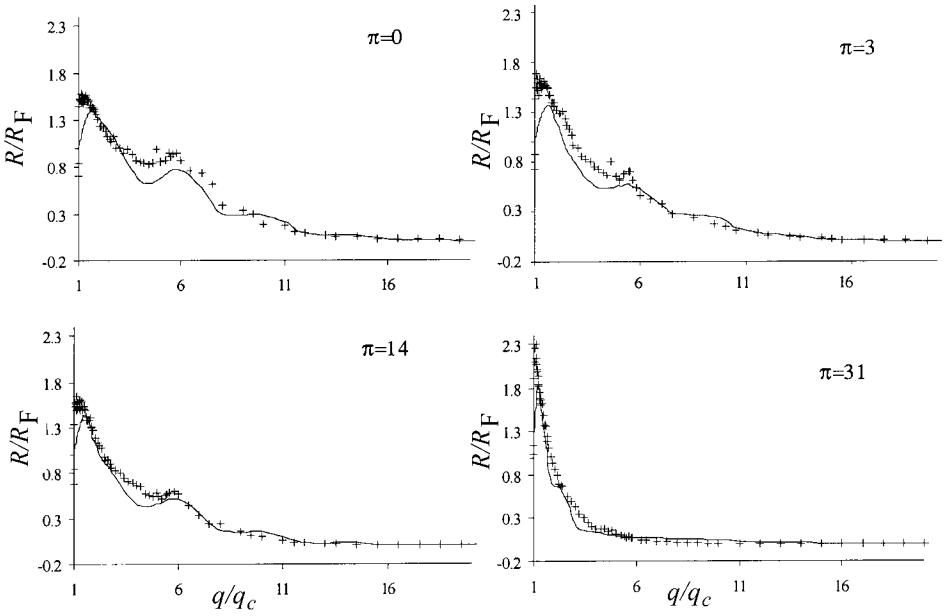

Fig. 5. *Measured* (+) *and calculated* (−) *X-ray-reflectivity curves of the [(l)-C_{22}Lys]$_2$CuPb film on aqueous subphase, at various surface pressures*

part of the film is in the form of a 5-Å-thick monolayer, in keeping with the rather low intensity of the *Bragg* peaks of the crystalline lattice.

The best fits (though not very good, they are shown here only as a guide to the interpretation) between the observed and calculated XR curves were obtained for 'patch' thickness of 5, 70, and 90 Å, with a refined surface roughness and relative surface coverage of each patch given in *Table 3*. The observed and calculated XR curves at four increasing surface pressures π [mN/m] are shown in *Fig. 5*. From this elaborate analysis, we observe that the relative surface coverage of the *ca.* 90-Å-thick domains increased from 20 to 39% upon compression, reaching $\pi = 14$ mN/m, with a concomitant decrease in the surface coverage of the 5- and *ca.* 70-Å-thick patches. The surface roughness of the *ca.* 90-Å-thick domains of $\sigma = 22$ Å^2 remained constant. The best fit for $\pi = 31$ mN/m was obtained for a surface coverage of 21% of the 90-Å patch thickness, and 66%, of 180-Å patch thickness. We rationalize this thickness in terms of a simple folding of the 90-Å layer at high surface pressure. This XR analysis, which is model-dependent, shows a buildup of surface coverage of the *ca.* 90-Å-thick layer that yielded the *W* peak.

Regarding the GIXD results that yielded 40-Å-thick crystallites according to the FWHM(q_z) of the (0,*k*) *Bragg* reflections, we tend to conclude from the XR analysis that the multilayer film does not contain patches *ca.* 40-Å-thick.

2.3. *Scanning-Force-Microscopy (SFM) Data*. SFM Measurements were performed on the [(*l*)-C_{22}Lys]$_2$CuPb film formed at the air−aqueous interface, which was compressed to +1 mN/m, and deposited on freshly cleaved mica. High-resolution phase images of the film clearly demonstrate the presence of a regular corrugation

Table 3. *Relative Surface Coverage* (in %) *and Roughness* σ (in Å^2) *of Film, Comprised of Patches of Different Thicknesses*[a]) (in Å) *at Various Surface Pressures* π (in mN/m) *That Best Fit the Measured X-Ray-Reflectivity Curves*

Patch thickness	$\pi = 0$		$\pi = 3$		$\pi = 14$		$\pi = 31$	
	%	σ	%	σ	%	σ	%	σ
5	48	5	50	5	38	7	13	7
70	32	6	20	6	24	6	–	–
91	20	22	30	22	39	22	21	22
180	–	–	–	–	–	–	66	25

[a]) The sum of the different patches of material was constrained to correspond to the total amount of deposited material.

observed on all islands deposited on mica (*Fig. 6,a*). The wavelength of the corrugation, averaging several such phase images, was calculated to be 55 Å (*Fig. 6,b*). This value is longer than the *d* spacing of the *W* peak (43 Å for [(*l*)-C_{22}Lys]$_2$CuPb; see *Table 1*) by almost 10 Å. This difference may be due to changes in the film upon transfer to the solid support. The topographic image of the film, despite significant noise, afforded a height analysis (see *Fig. 6,b*) of a regular corrugation, with vertical amplitude of minimally 4 Å (*Fig. 6,c*).

2.4. *Various Models That May Not Account for the* W *Peak*. The *W* peak may arise from an additional phase, with a *d* spacing of *ca.* 41.5 Å. The calculated lengths of the all-*trans* bolaamphiphilic molecules forming the multilayer crystalline films are 31.5 Å for C_{22}Orn, and 32.5 Å for C_{22}Lys. Complexation with Cu^{2+} and Pb^{2+} yields a calculated chain axis repeat of 73.5 Å and 76.0 Å, respectively. The observed lattice *d* spacings from the GIXD measurements are *ca.* 70 and *ca.* 73 Å, respectively (see *Table 1*), corresponding to molecular chains lying parallel on the H_2O surface, and tilted by *ca.* 16° from the normal to the plane of the metal-ion sheets (see *Fig. 1,b*).

To obtain an additional phase with *ca.* 41.5-Å spacing, the chain would have to be tilted by *ca.* 55° from the normal to the layer spacing, = acos (*ca.* 41.5 Å/maximal-length), as depicted in *Fig. 7,a*. Such a large tilt would lead to an offset of *ca.* 6 Å, = 4.1/tan35°, between the neighboring chains, where 4.1 Å is the interchain spacing obtained from GIXD, which may disrupt favorable interactions between the head-groups and reduce hydrophobic intermolecular contacts. Most importantly, such an arrangement should lead to higher-order reflections, which were not observed.

A second possibility is the incorporation into the structure of CH_3COOH molecules present in the subphase. Such a model would lead to a cell comprising the two bolaamphiphiles, and two CH_3COOH molecules forming a salt with a Pb^{2+} cation, in a head-to-head and tail-to-tail arrangement (*Fig. 7,b*). The fully stretched length of such a repeat would be *ca.* 85 Å, depending on the organic spacer, half of which is close to the *d* spacing of the *W* peak. However, on the basis of the XPS experiments, where a ratio of 1:1 between Pb and Cu was found [11], this model may be dismissed.

A third possibility may be that the *W* peak arises from a phase where the chains are in partial misregistry in the direction of the long molecular axis, which would diminish the intensities of higher-order reflections. However, it is difficult to envisage that individual bolaamphiphile-cation polymers will not be arranged in lateral registry

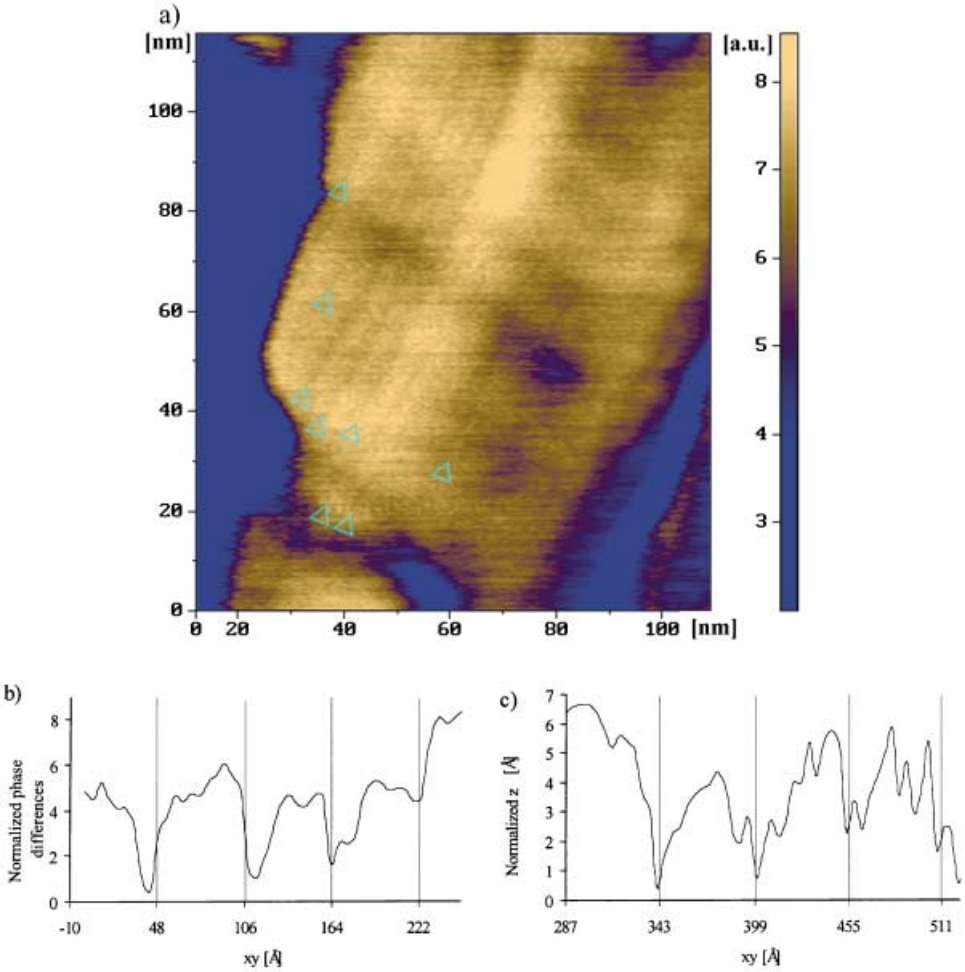

Fig. 6. *SFM Studies showing regular corrugation on a mica-deposited film of [(1)-C_{22}Lys]$_2$CuPb on an aqueous subphase of mixed Cu(Ac)$_2$ and Pb(Ac)$_2$, and compressed to +1 mN/m.* Examples of a typical patch: *a*) phase image; *b*) and *c*) corresponding phase-image cross-sections.

(*Fig. 1,b*), *i.e.*, within one layer, particularly when an amide moiety is present to induce H-bonding between chains.

The measured X-ray-reflectivity (XR) curves could not be interpreted in terms of a film of single thickness. The reflectivity curves were modeled assuming the film to be composed of patches of different thickness. In the light of the results analyzed, we postulate, tentatively, that the 40- and 90-Å thicknesses estimated from the GIXD data belong to the same crystalline phase, where the *W* peak arises from periodic corrugation.

2.5. *Proposed Model of the Corrugated Structure.* Here, we interpret the *W* peak as arising from a periodic variation in electron density parallel to the H_2O surface along

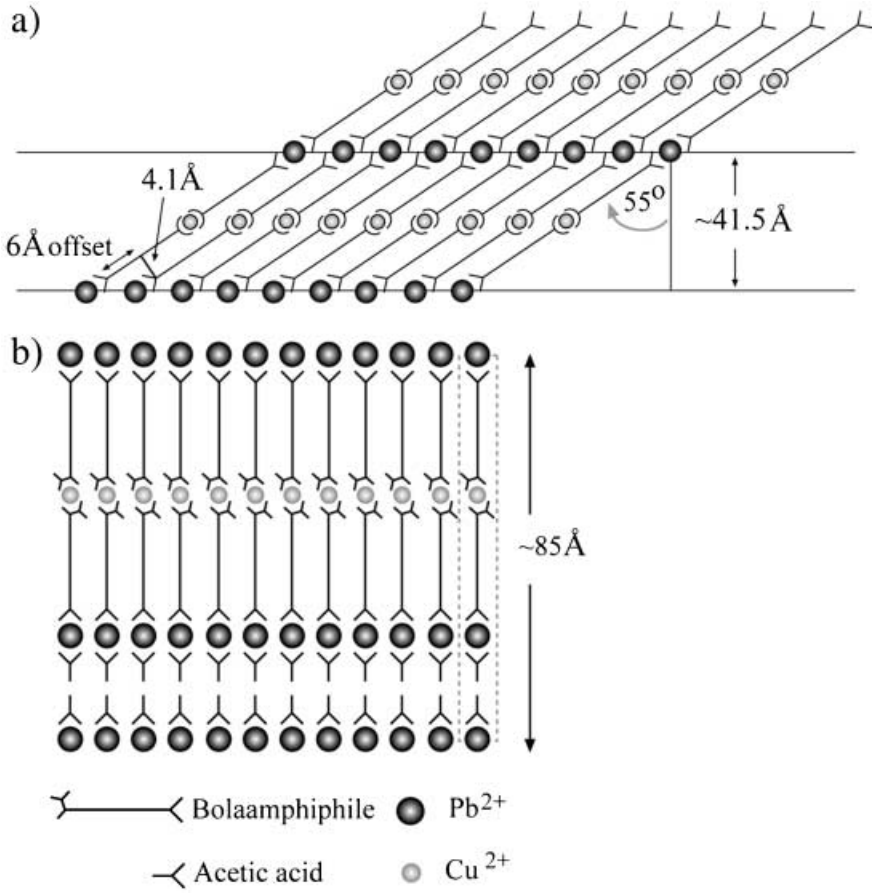

Fig. 7. *A top-view representation of two packing arrangements corresponding to crystalline phases in disagreement with the experimental data:* a) *a phase whose molecular chains are tilted by 55° from the normal to the layer spacing*; b) *a phase incorporating CH_3COOH molecules in the crystalline structure*

the direction of postulated corrugation. To construct such a model with a d_w spacing of *ca.* 41.5 Å, but built from the multilayer crystalline film shown in *Fig. 1,b* and *c*, we conceive a super cell composed of block crystallites of 90-Å height and length corresponding to that of the d_w spacing, extending in the *x* direction (*Fig. 1,b*) along which the molecular chains are stacked. To achieve the necessary variation of in-plane electron density, the block crystallites juxtaposed along the *x* direction were tilted by an angle τ *vis-à-vis* the H_2O surface to form a corrugated superstructure. Two models were considered, labeled 'saw-tooth' (*Fig. 8,a*) and the 'zig-zag' (*Fig. 8,b*). In both models, the angle τ was first set at 3°, since it was reported that multilayers of Cd^{2+} salt of docosanedioic acid make such an angle with the water surface [13]. The two models constructed from $[(l)\text{-}C_{22}Lys]_2CuPb$ molecular chains were tested with the SHELX97 X-ray structure-factor program [18][19] to establish the general possibility of obtaining a *W Bragg* peak, with the correct shape of the *Bragg* rod-intensity profile along q_z.

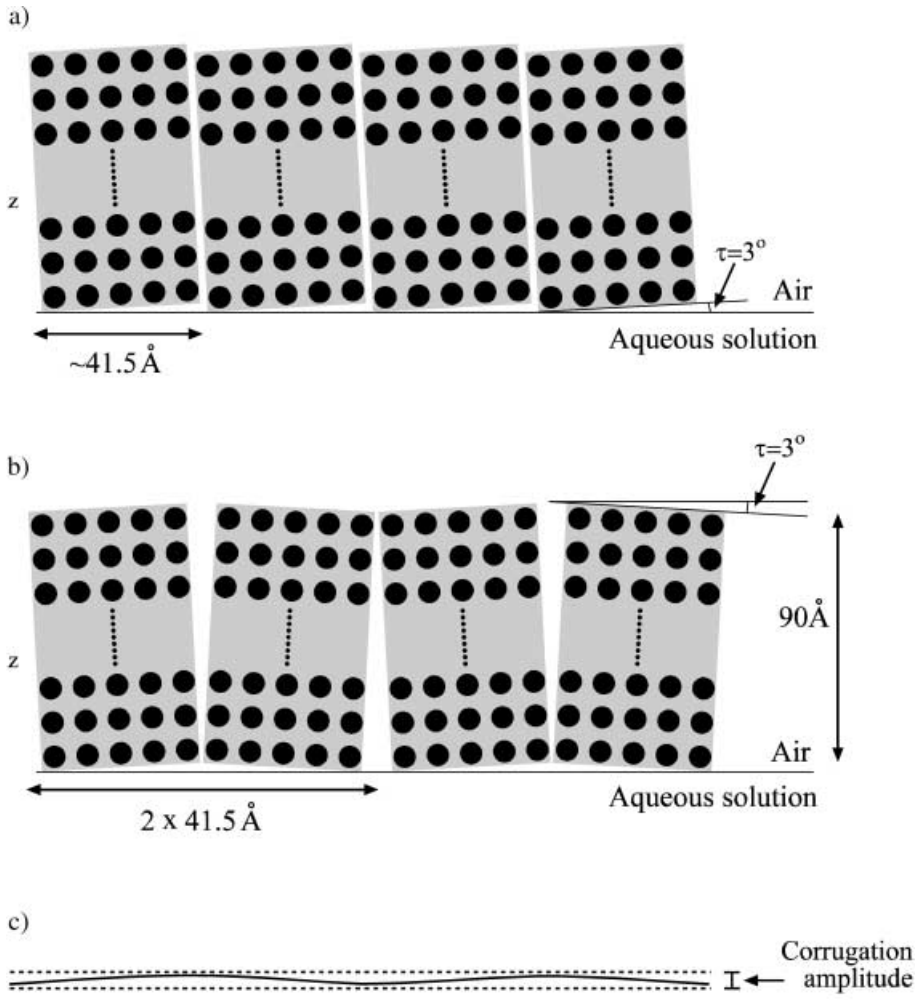

Fig. 8. *A representation of* a) *saw-tooth and* b) *zig-zag models used for molecular simulation viewed parallel to the long molecular axis, as well as* c) *the topographical corrugation amplitude corresponding to the zig-zag model.* Filled circles represent molecules.

The 43.1-Å d_w spacing of the [(*l*)-C_{22}Lys]$_2$CuPb film *W* peak (see *Table 1*) is not a precise multiple of the 4.1-Å interchain spacing. We may rationalize this mismatch, not as a result of the difficulty in determining the precise centers of the *Bragg* peaks corresponding to the two relevant reflections, but rather because the model does not require a precise fit. Indeed, the lack of higher-order reflections suggests that the structural repeat along the direction of corrugation should be imperfect. X-Ray-structure-factor calculations for the 'saw-tooth' model (*Fig. 8,a*) yielded a calculated *Bragg* rod whose intensity maximum is at a much higher value than at the observed q_z value of 0 Å^{-1}, and was, therefore, discarded. The calculated *Bragg* rod from the 'zig-zag' model (*Fig. 8,b*), shown in *Fig. 9,b*, gave a reasonable fit to that of the observed

Bragg rod (*Fig. 9,b*). Here, we note that the 'zig-zag' model incorporates a (pseudo)-plane of symmetry perpendicular to the water surface resulting in a calculated *Bragg* rod that peaks at the observed value of 0 $Å^{-1}$. *Fig. 9,a* shows a very weak calculated *Bragg*-rod profile for double the *d* spacing of the *W* peak, whereas the *Bragg* rod corresponding to the *W* peak (*Fig. 9,b*) is intense, in agreement with observation. All the other calculated *Bragg* rods for odd harmonics of the *W* peak were extremely weak, whereas calculated even-order harmonics gave gradually decreasing intensities. The absence of the latter in the GIXD pattern implies poor in-plane order for the corrugated structure, in keeping with its low number of four repeat units, as determined by $L/2d_w$ (*ca.* 300/83), where *L* is the coherence length along the corrugation direction (*Table 2*) and $2d_w$ the translation repeat (*Fig. 8,b*).

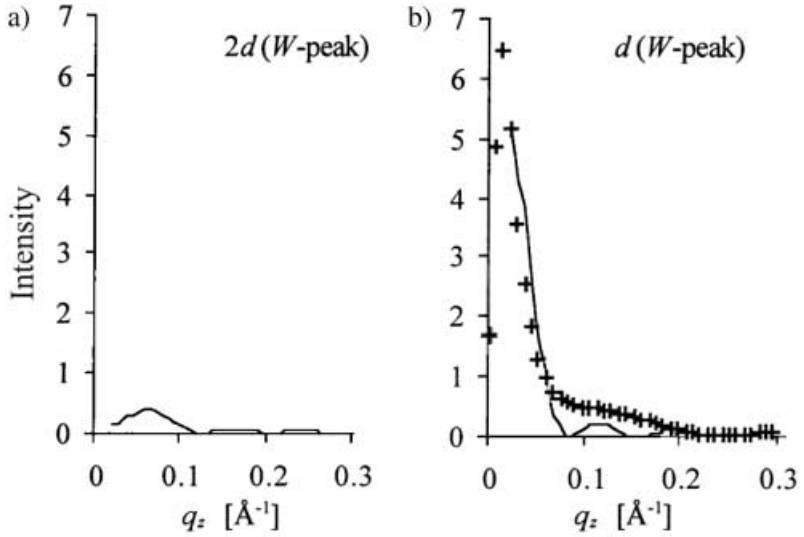

Fig. 9. *Calculated* Bragg-*rod-intensity profiles* (line) *along* q_z *of the first- and second-order reflections, with spacings* a) $2d_w$ *and* b) d_w (=41.5 Å), *respectively, corresponding to the 'zig-zag' model* (*Fig. 3,b*). The measured *Bragg*-rod-intensity profile (+) of the *W* peak is shown in *b*.

We examined other factors contributing to the *Bragg*-peak intensity in the 'zig-zag' model. The results show that, on increasing the tilt angle τ from the set value of 3°, the intensity of the *W* peak is enhanced. Naturally, on reducing the number of layers in the vertical direction, the intensity of the *Bragg* peak is reduced. Both factors contribute to enhancement of the electron-density variation in the direction of corrugation.

We propose a simple structural model accounting for the difference in FWHM(q_z) of the *W Bragg* peaks, indicating a film thickness of *ca.* 90 Å and the FWHM(q_z) of the (0,*k*) reflections corresponding to a crystal thickness of *ca.* 40 Å: it involves a lateral misregistry primarily along the *b* direction (*i.e.*, parallel to the molecular-chain axis) between vertically stacked crystalline blocks that would affect the FWHM(q_z) of the (0,*k*) reflections, but not that of the *W Bragg* rod, since the direction of misregistry between the crystalline blocks is orthogonal to the proposed direction of corrugation. One drawback of the model is to reconcile the non-skewed shape of the *W Bragg* rod

along q_t $(=q_{xy}^2 + q_z^2)^{1/2}$ with the skewed *Bragg* rod corresponding to the 4.1-Å spacing of the regular crystalline multilayer (see *Fig. 2*), the latter interpreted in terms of a film bent about the *y* axis shown in *Fig. 1,b*, discussed in *Sect. 2.1*. We assume that the ordered part of the corrugated film occupies the horizontal central section of the bent multilayer.

3. Concluding Remarks. – A detailed analysis supports the presence of regular anisotropic corrugation forming a superstructure of the metal complexes of the long-chain bifunctional bolaform amphiphiles $[C_{22}Orn]_2CuPb$ and $[C_{22}Lys]_2CuPb$ that form crystalline multilayer films. This proposed corrugation is an intrinsic feature of the film found in the uncompressed state, and is retained on transfer to a solid support, as detected by SFM phase images. The corrugation is parallel to the air–aqueous interface, extending for about five to seven repeat units, occurring in a direction normal to that of the cation planes, approximately parallel to the long hydrocarbon chain.

The absence of higher-order reflections of the *W* peak implies low lateral order for the corrugated model structure[3]). The vertical variation in amplitude at the surface of the corrugated structure is likely to be less than a nm, in keeping with the topographic SFM measurements and model analysis.

We were led by a process of elimination to the proposed model that the corrugated structure is a supramolecular arrangement incorporating the established multilayer crystalline films of the $[C_{22}Orn]_2CuPb$ or $[C_{22}Lys]_2CuPb$ bolaamphiphilic cation chains: first, we could not devise any regular arrangement of the bolaamphiphilic chains to satisfy the *d* spacing of the *W* peak, particularly with the constraint of low lateral order. No less important, we could not conceive of any superstructure that would not incorporate a regular arrangement of the bolaamphiphilic cation chains as a sublattice, namely the observed regular crystalline phase. Furthermore, we had not been able to produce a reasonable model that incorporates a superstructure with a variation in in-plane electron density without the corrugation that manifests in the *z* direction. To achieve this corrugated state, it was necessary to tilt the multilayer plane away from that of the water surface. This tilt reduces the unfavorable interactions between the polar aqueous surface and the nonpolar hydrocarbon chains of the bolaamphiphiles.

The formation of crystalline corrugation appears to be an intrinsic feature of the film, but one that is difficult to predict. Several other systems have been checked, but they did not reveal corrugation, which must be periodic to be manifest[4]).

---

[3]) Here, we note that the corrugated structure of cadmium stearate – studied by *Daillant* and co-workers – also yielded only one low-order diffraction peak [5][6]. However, the similarity of this system to that studied is remote, since the former consists of a monolayer in which the organic molecules lie perpendicular to the aqueous surface, whereas, in the present case, the film consists of a multilayer in which the bolaamphiphiles lie parallel to the air–aqueous interface.

[4]) To search for other examples of corrugated films, we have examined by GIXD monolayers of $C_{50}H_{32}$ paraffin and N–$C_{29}H_{58}$–(*l*)-CONH–$(CH_2)_4$–CH(COOH)(NH_2), on H_2O, as well as multilayers of tetracosanedioic acid on 1 mM $Pb(NO_3)_2$, and *N,N*–(*l*)-(NH_2)(COOH)CH–$(CH_2)_4$–CONH–$C_{14}H_{25}$–(*l*)-CONH–$(CH_2)_4$–CH(COOH)(NH_2) on 1 mM $Cu(Ac)_2$ for the presence of long-wavelength corrugation, all down to $q_{xy} = 0.9$ Å^{-1} ($d = 83$ Å), but to no avail.

Experimental Part

General. The bolaamphiphiles (*l*)- or (*d,l*)-C_{22}Orn, and (*l*)- or (*d,l*)-C_{22}Lys (*Fig. 1,a*) were synthesized as described in [11]. The $Pb(Ac)_2$ and $Cu(Ac)_2$ salts were purchased from *Sigma-Aldrich* in 99.999% purity. Millipore pure H_2O (18.2 MΩ) was used to prepare the subphase solutions. $CHCl_3$ and CF_3COOH (TFA), both anal. grade, were purchased from *Merck* and *Sigma-Aldrich*, resp.

1. *Film-Formation Procedure*. The crystalline films of (*l*)- or (*d,l*)-$[C_{22}Orn]_2CuPb$, and (*l*)- or (*d,l*)-$[C_{22}Lys]_2CuPb$ (*Fig. 1,a*) were prepared by spreading solns. of the bolaamphiphiles (*l*)- or (*d,l*)-C_{22}Orn, and (*l*)- or (*d,l*)-C_{22}Lys (0.4 mM amphiphile dissolved in $CHCl_3$ with 2% TFA) at r.t., over aq. soln. containing an equimolar mixture of $Pb(Ac)_2$ and $Cu(Ac)_2$ (1 mM each) in a *Teflon* trough.

2. *Grazing-Incidence X-Ray Diffraction and X-Ray-Reflectivity Experiments*. The GIXD and specular XR measurements were made on the liquid-surface diffractometer at beamline BW1 in *HASYLAB* at *DESY*, Hamburg, Germany. After the film was prepared (see above), the trough container was closed, purged with 4° cold He gas, and cooled to 4° before X-ray measurements were performed. The scattered-X-ray intensity was detected by a position-sensitive detector (PSD) equipped with *Soller* slits. This detector resolves the vertical component of the X-ray-scattering vector $q_z \approx (2\pi/\lambda)\sin\alpha_f$, α_f being the angle between the plane of the liquid surface and the diffracted beam, and $\lambda = 1.30$ Å. The q_{xy} resolution is limited to that of the *Soller* slits. Each sample consists of 2D crystallites that are randomly oriented *vis-à-vis* the normal to the soln. surface, and, thus, is a '2D powder'. Measurements were performed by scanning the horizontal scattering vector $q_{xy} \approx (4\pi/\lambda)\sin\theta_{xy}$, where $2\theta_{xy}$ is the angle between the incident and diffracted beams projected onto the horizontal plane.

The GIXD data are represented as a 2D intensity-distribution plot, showing the scattered intensity $I(q_{xy},q_z)$ as a function of q_{xy} and q_z. The q_{xy} positions of the *Bragg* peaks yield the lattice-repeat distances $d = 2\pi/q_{xy}$, which can be indexed by two indices (h,k) to yield the unit cell. The full width at half maximum (FWHM(q_z)) of the *Bragg*-rod-intensity profiles along q_z yields a first estimate of the crystallite thickness according to the *Scherrer* formula [16] $L_z = 0.88 \cdot 2\pi/\mathrm{FWHM}(q_z)$, or half this value for *Bragg* rods that peak at $q_z = 0$ Å^{-1}.

More quantitatively, the intensity at a particular q_z value in a (h,k) *Bragg* rod is determined by the square of the molecular structure factor $|F_{hk}(q_z)|^2$, thus allowing its evaluation according to an atomic-coordinate model of the molecules [12].

The XR experiment was performed directly after GIXD measurements for a particular compression of the film. The experiments were performed by scanning the incident angle (α_i), equal to the reflected angles α_f, from 0.5 α_c to 40 α_c where α_c is the critical angle for total external reflection of X-rays from H_2O. The reflected X-rays were detected by a NaI scintillation counter. The experimental results are given in the form of a normalized X-ray reflectivity R/R_F, in which R_F is the '*Fresnel*' reflectivity calculated for a perfect sharp interface as a function of the normalized vertical scattering vector q_z/q_c, where $q_z = (4\pi/\lambda)\sin(\alpha_i)$ and $q_c = (4\pi/\lambda)\sin(\alpha_c) = 0.0276$ Å^{-1} is the scattering vector at the critical angle of incidence.

3. *Scanning-Force Microscopy (SFM)*. The films were prepared at r.t. in a small *Teflon* trough [20], which was subsequently closed and cooled to 4°. After 30 min, the film was compressed to +1 mN/m, and the H_2O was slowly drained, resulting in deposition of the film on freshly cleaved mica pieces that were *a priori* immersed in the aq. subphase. The dry film was used for the SFM experiments, which were conducted on an *NT-MDT P47 Solver*, in semicontact mode with *NSC12* probes (*Micromasch*) with resonance frequencies ranging between 50 and 280 kHz. XY Spacing was calibrated with a grid with 200-nm spacing (*Nanosensors*) and *Z* calibration made on a 25-nm height grid (*NT-MDT*). Both topographic (tapping mode) and phase images were acquired, the latter showing the striped features more clearly.

4. *Construction of the Models Proposed for the Corrugated Structure*. Two models displaying crystalline superstructures, 'saw-tooth' and 'zig-zag' (*Fig. 8,a* and *b*), were constructed with the CERIUS^2 computational package (*Accelrys*, San Diego. CA). The models were then used in structure-factor calculations making use of the SHELX97 X-ray structure-factor program [18][19], yielding *Bragg*-rod-intensity profile along q_z.

The following procedure was adopted for the application of SHELX97 computer program (designed for 3D crystals) to calculate *Bragg*-rod-intensity profile of a multilayer crystal in form of a 2D powder, randomly oriented around the normal to the surface. The *Bragg*-rod intensities $F^2(h,k,q_z)$ were assigned *l Miller* indices according to a virtual *c* axis ($c = 2\pi/\Delta q_z$) to transform a continuous $F^2(h,k,q_z)$ distribution along q_z into a discrete $F^2(h,k,l)$ reflection data set corresponding to the virtual 3D crystal. The superposition of the $F^2(h,k,q_z)$ and $F^2(-h,-k,q_z)$ *Bragg* rods, a property of the measured GIXD pattern since the sample on H_2O consists of a 2D crystalline 'powder', was simulated in SHELX97 by imposing a twinning of the crystal about the *ab* plane [17a].

Note that the SHELX97 program used allows for a maximum of 10000 atoms in the asymmetric unit cell. Within these limitations, we assumed a repeat unit containing eight $[C_{22}Lys]_2CuPb$ molecules in the horizontal

direction (x) and 17 molecules in the vertical direction (z), spaced 5 Å apart in both x and z directions. The repeat unit ($a = 45$, $b = 78.5$, $c = 85$ Å, where b indicates the length of one $[C_{22}Lys]_2CuPb$ molecule) was tilted by $\tau = 3°$ from the air–solution interface (*Fig. 8*).

For the 'saw-tooth' model, we assumed a simple unit repeat along the x direction (*Fig. 8,a*), where 45 Å represents the d-spacing of the W peak. For the 'zig-zag' model, we constructed an arrangement (*Fig. 8,b*) comprising mirror symmetry perpendicular to the x direction, with a unit-cell repeat of 93 Å along x, the $2d$ spacing of the W peak. In this model, a void is present, which may partially accommodate disordered molecules, not contributing to the crystallinity.

We thank the *Binational Science Foundation USA–Israel* for financial support.

REFERENCES

[1] L. J. W. Shimon, M. Vaida, L. Addadi, M. Lahav, L. Leiserowitz, *J. Am. Chem. Soc.* **1990**, *112*, 6215.
[2] A. Tardieu, V. Luzzati, F. C. Feman, *J. Mol. Biol.* **1973**, *75*, 711.
[3] R. W. Date, G. R. Luckhurst, M. Shuman, J. M. Seddon, *J. Phys. Il France* **1995**, *5*, 587.
[4] J. T. Woodward, J. A. Zasadzinski, *Phys. Rev. E* **1996**, *53*, R3044.
[5] C. Fradin, J. Daillant, A. Braslau, D. Luzet, M. Alba, M. Goldmann, *Euro. Phys. J. B* **1998**, *1*, 57.
[6] J. Daillant, *Synchrotron Radiation News* **1999**, *12*, 17.
[7] L. Bourdieu, J. Daillant, D. Chatenay, A. Braslau, D. Colson, *Phys. Rev. Lett.* **1994**, *72*, 1502.
[8] P. Fontaine, J. Daillant, P. Guenoun, M. Alba, A. Braslau, J.W. Mays, J.-M Petit, F. Rietourd, *J. Phys. II France* **1997**, *7*, 401.
[9] J. A. Zasadzinski, R. Viswanathan, D. K. Schwartz, J. Garnaes, L. Madsen, S. Chiruvolu, J. T. Woodward, M. L. Longo, *Colloids. Surf., A* **1994**, *93*, 305.
[10] M. A. Dvorak, S. L. Li, M. D. Ward, *Chem. Mater.* **1994**, *6*, 1386.
[11] R. Buller, H. Cohen, T.R. Jensen, K. Kjaer, M. Lahav, L. Leiserowitz, *J. Phys. Chem. B* **2001**, *105*, 11447.
[12] D. Jacquemain, S. Grayer-Wolf, F. Leveiller, M. Deutsch, K. Kjaer, J. Als-Nielsen, M. Lahav, L. Leiserowitz, *Angew. Chem., Int. Ed.* **1992**, *31*, 130.
[13] I. Weissbuch, S. Gou, R. Edgar, S. Cohen, P. B. Howes, K. Kjaer, J. Als-Nielsen, M. Lahav, L. Leiserowitz, *Adv. Mater.* **1998**, *10*, 117.
[14] V. Hensel, A. Godt, R. Popovitz-Biro, H. Cohen, T. R. Jensen, K. Kjaer, I. Weissbuch, E. Lifshitz, M. Lahav, *Chem.–Eur. J.* **2002**, *8*, 1413.
[15] J. Majewski, R. Edgar, R. Popovitz-Biro, K. Kjaer, W. G. Bouwman, J. Als-Nielsen, M. Lahav, L. Leiserowitz, *Angew. Chem., Int. Ed.* **1995**, 34, 649.
[16] A. Guinier, 'X-Ray Diffraction', W. H. Freeman & Co., San Francisco, 1963, p. 121–125.
[17] a) H. Rapaport, I. Kuzmenko, S. Lafont, K. Kjaer, P. B. Howes, J. Als-Nielsen, M. Lahav, L. Leiserowitz, *Biophys. J.* **2001**, 81, 2729; b) K. Y. C. Lee, J. Majewski, T. L. Kuhl, P. B. Howes, K. Kjaer, M. M. Lipp, A. J. Waring, J. A. Zasadzinski, G. S. Smith, *Biophys. J.* **2001**, 81, 572.
[18] G. M. Sheldrick, 'SHELXL97 Program for the Refinement of Crystal Structures', University of Göttingen, Germany, 1997.
[19] G. M. Sheldrick, *Acta Crystallogr., Sect. A* **1990**, *46*, 467.
[20] J. Majewski, L. Margulis, I. Weissbuch, R. Popovitz-Biro, T. Arad, Y. Talmon, M. Lahav, L. Leiserowitz, *Adv. Mater.* **1995**, *7*, 26.

Received June 6, 2003